BOLETIN DE LA SOCIEDAD ESPAÑOLA DE
Cerámica y Vidrio
www.elsevier.es/bsecv

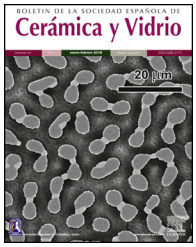

Neodymium doped lanthanide fluoride nanoparticles as contrast agents for luminescent bioimaging and X-ray computed tomography

Daniel González-Mancebo[a], *Ana I. Becerro*[a], *Roxana M. Calderón-Olvera*[a], *Eugenio Cantelar*[b], *Ariadna Corral*[c,d], *Marcin Balcerzyk*[c,d], *Jesús M. de la Fuente*[e], *Manuel Ocaña*[a,*]

[a] *Instituto de Ciencia de Materiales de Sevilla (CSIC-US), c/Américo Vespucio, 49, 41092 Seville, Spain*
[b] *Depto. Física de Materiales, Universidad Autónoma de Madrid, c/Francisco Tomás y Valiente no. 7, 28049 Madrid, Spain*
[c] *Centro Nacional de Aceleradores (Universidad de Sevilla-CSIC-Junta de Andalucía), c/Thomas Alva Edison 7, 41092 Sevilla, Spain*
[d] *Departamento de Fisiología Médica y Biofísica, Facultad de Medicina, Universidad de Sevilla, Avenida Sánchez Pizjuán 4, 41009 Sevilla, Spain*
[e] *Instituto de Nanociencia y Materiales de Aragón, CSIC/University of Zaragoza, and CIBER-BBN, Edificio I+D, c/Mariano Esquillor s/n, 50018 Zaragoza, Spain*

ARTICLE INFO

Article history:
Received 29 April 2021
Accepted 15 July 2021
Available online 23 October 2021

Keywords:
Neodymium
Lanthanum fluoride
Nanoparticles
Luminescence
Computed tomography
Cytotoxicity

ABSTRACT

The synthesis of uniform neodymium-doped lanthanum trifluoride nanoparticles with lenticular shape and a mean diameter around 45 nm by using a homogeneous precipitation method is reported. The luminescent properties of the synthesized samples in terms of their emission spectra and emission lifetime are analyzed as a function of the Nd content to find the optimum phosphor and its suitability for luminescent imaging in the second biological window. The X-ray attenuation properties of the optimum phosphor are evaluated to investigate their additional ability as contrast agent for X-ray computed tomography. Finally, the colloidal stability of the obtained nanoparticles in physiological medium and their cytotoxicity are also analyzed to assess their aptness for *in vivo* bioimaging applications.

Nanopartículas de fluoruro de lantano dopadas con neodimio como agentes de contraste para bioimagen mediante luminiscencia y tomografía computarizada de rayos X

Palabras clave:
Neodimio
Fluoruro de lantano

RESUMEN

En este trabajo se ha desarrollado un método de síntesis de nanopartículas uniformes de trifluoruro de lantano dopadas con neodimio, con forma lenticular y un diámetro medio en torno a 45 nm, basado en un proceso de precipitación homogénea en medio acuoso. Las

* *Corresponding author.*
E-mail address: mjurado@icmse.csic.es (M. Ocaña).
https://doi.org/10.1016/j.bsecv.2021.07.004

Nanopartículas
Luminiscencia
Tomografía computarizada
Citotoxicidad

propiedades luminiscentes de las muestras sintetizadas en términos de sus espectros de emisión y tiempo de vida de las emisiones se han analizado en función del contenido de neodimio (Nd) para determinar el nanofósforo óptimo y su idoneidad para la obtención de imágenes luminiscentes en la segunda ventana biológica. Asimismo, se han evaluado las propiedades de atenuación de rayos X del nanofósforo óptimo para valorar su capacidad adicional como agente de contraste para tomografía computarizada de rayos X. Por último, también se han analizado la estabilidad coloidal de las nanopartículas obtenidas en medio fisiológico y su citotoxicidad para determinar su aplicabilidad para la obtención de imágenes biológicas *in vivo*.

Introduction

Phosphors based on lanthanum trifluoride (LaF_3) doped with lanthanide cations (Ln^{3+}) (Ln:LaF_3) have been widely investigated owing to their excellent luminescent properties arising from the low energy phonons of the LaF_3 matrix, which involves a low probability of luminescence quenching by phonon-assisted nonradiative decay [1]. Because of such properties, this kind of phosphors has been proposed for several applications including lighting [2], anti-counterfeiting [3], sensing [4,5], thermometry [6,7], therapy [8–10], bioimaging [11–13] and theranosis [14]. For the latter application, the Nd^{3+}:LaF_3 system is of particular interest since the excitation (~800 nm) and main emission (~1060 nm) wavelength of the Nd^{3+} cations lie in the near-infrared (NIR) region within the so-called biological window I (650–950 nm) and II (1000–1350 nm), respectively, in which undesired effects such as absorption and scattering of radiation by tissues are minimized and the radiation penetration depth is high [15]. It is also worth mentioning that X-ray computed tomography (CT) is a powerful imaging technique used in biomedical diagnosis that frequently requires the use of contrast agents (CAs). CT contrast increases with increasing atomic number (*Z*) of the elements that make up the CA [16]. The main CT CAs used nowadays are compounds based on iodine ($Z = 53$) and barium ($Z = 56$), which show lower *Z* values than any lanthanide element (from 57 to 71). Therefore, Nd-doped LaF_3 might behave as a dual probe for both, luminescent bioimaging and CT. The use of this kind of dual probes would avoid the administration of different, specific CAs for each technique thus minimizing their possible adverse effects.

It is important to note that particulate CAs for *in vivo* biomedical applications must meet some specific requirements [17,18]. First, the particles must present a uniform size between 20 and 100 nm to avoid embolism and the nanoparticles (NPs) premature elimination, since smaller NPs are quickly eliminated through the kidney and larger NPs, by the mononuclear phagocyte system. Second, NPs aggregation in the physiological environment should be avoided to meet the above size criteria, and finally, it is obvious that the NPs must be biocompatible (lack of cytotoxicity).

Up to now, several procedures have been developed to synthesize Nd^{3+} doped LaF_3 NPs, most of which are based on wet chemistry routes, specifically, hydrothermal/solvothermal methods in the absence [11,19] or the presence [12,20–23] of organic additives acting as capping or dispersing agents. Among these methods, only that reported by Cheng et al. [8], based on the use of oleic acid (OA) as a capping agent succeeded in producing uniform NPs. However, they presented hydrophobic character, as a consequence of the presence of OA moieties on the NPs surface, which precludes their use for bioapplications. Therefore, the search for synthesis procedures yielding monodisperse Nd:LaF_3 NPs colloidally stable in physiological media is still challenging.

In this paper, a very simple room temperature procedure is reported, which produces uniform and hydrophilic NPs colloidally stable in saline medium. The luminescent properties of these NPs are evaluated as a function of the Nd doping level to find the most efficient phosphor. The X-ray attenuation properties of this system are also analyzed in comparison with a commercial CT CA for the first time in literature. Finally, cytotoxicity experiments are also shown aiming to investigate the suitability of the here reported Nd:LaF_3 NPs for luminescent and CT bioimaging.

Experimental

Reagents

Ethylene glycol (anhydrous, Sigma Aldrich, 99.8%), lanthanum nitrate ($La(NO_3)_3{\cdot}6H_2O$, Sigma Aldrich, 99%), neodymium nitrate ($Nd(NO_3)_3{\cdot}6H_2O$, Sigma Aldrich, 99.9%), sodium tetrafluoroborate ($NaBF_4$, Sigma Aldrich, 98%), Iohexol (Sigma Aldrich, analytical standard, ≥95%) and saline medium (physiological serum 0.9% NaCl, B. Braun 250 mL) were used as received.

Synthesis of nanoparticles

Nd-doped LaF_3 NPs were synthesized following a method similar to that previously developed by us for the synthesis of europium–bismuth codoped LaF_3 [13]. Briefly, two different solutions were prepared with magnetic stirring at room temperature for 2 h. One of them containing lanthanum and neodymium nitrates in 3 mL of an ethylene glycol/water mixture (90/10 by volume), and the other one containing sodium tetrafluoroborate (0.36 mol/dm^3) dissolved in 3 mL of the same solvents mixture. Both solutions were admixed together and kept under stirring for a couple of minutes to achieve a good homogenization and then aged at room temperature

for 2 h. The final concentration of lanthanides was kept constant ([La] + [Nd] = 0.1 mol/dm^3) and the Nd/(La + Nd) mol% was varied from 0.25% to 2.0%. The resulting suspension was centrifuged and the precipitates washed, twice with ethanol and once with double distilled water. The so obtained particles were dispersed in distilled water or dried at 50 °C for some analyses.

Characterization techniques

Transmission electron microscopy (*TEM*, JEOL2100Plus) was used to examine the shape and size of the nanoparticles. Particle size distributions were obtained from the micrographs by counting several hundreds of particles, using the free software *ImageJ*. Dynamic light scattering (DLS) was used to obtain additional information about size and colloidal stability of the nanoparticles, both in aqueous and saline solution (0.5 mg/cm^3 of solid). The experiments were carried out using a Malvern Zetasizer Nano-ZS90 equipment, which was used as well to measure the Zeta potential of the suspensions.

The crystalline structure of the prepared nanoparticles was assessed by X-ray diffraction (XRD) using a Panalytical X'Pert Pro diffractometer (Cu Kα) with an X-Celetor detector over an angular range of $5^\circ < 2\theta < 120^\circ$ 2θ, 0.02° step width, and 600 s counting time. Lattice parameters of the LaF_3 crystal structure were calculated using the Rietveld method with the TOPAS software (TOPAS version 4.2, Bruker AXS, 2009). The parameters refined were: zero of the diffractometer, background coefficients, scale factor, lattice parameters and profile parameters.

The composition of Nd-doped LaF_3 nanoparticles was determined by inductively coupled plasma (ICP) using ICP-AES Horiba Jobin Yvon, Ultima 2 apparatus. Nanoparticles were previously digested with a small amount of hydrochloride acid.

The photoluminescence of the Nd-doped LaF_3 nanoparticles, in powder form, was analyzed by measuring excitation and emission spectra recorded using a CW diode laser @ 810 nm as excitation source and an ARC monochromator model SPectraPro 500i with an AsGaIN photodiode, to detect fluorescent emission. The powder samples were placed filling a tiny hole (3 mm diameter) practiced in an aluminum foil and sandwiched between two microscope slides.

Nd^{3+} decay curves for the $^4F_{3/2} \rightarrow {}^4I_{11/2}$ transition (at 1056 nm) were obtained under pulsed excitation using a MOPO @λ_{exc} = 810 nm with a pulse width of 10 ns and 10 Hz repetition rate. The curves were averaged by a Tektronix DPO4104B-L digital oscilloscope.

For the evaluation of the CT contrast efficiency, aqueous dispersions containing different concentration of the Nd-doped LaF_3 nanoparticles and a commercial CT CA (Iohexol) were prepared. Then, an aliquot (200 μL) of each suspension, previously stirred for 2 min, was placed in a multiwell microplate along with a Milli-Q water sample as reference for calibration. X-ray attenuation measurements were carried out in a NanoSPECT/CT (Bioscan) using the following acquisition parameters: 106 mA current for a 75 kV voltage, exposure time per projection of 1500 ms and 360 projections per rotation. The final length image was 6 cm with a total acquisition time of 18 min. The image was reconstructed with Vivoquant image processing software (Invicro), with the exact cone-beam filtered back-projection algorithm and the Shepp Logan 98% filter. Finally, the images were analyzed by PMOD 3.8 software (PMOD Technologies LLC) and a spherical volume of interest (VOIs) of 2 mm radius was made within each sample to calculate the X-ray attenuation (in Hounsfield Unit, HU) for each concentration. The final images were represented in a greyscale.

Cell viability was determined using an MTT colorimetric assay. Vero cells were growth in a Dulbecco's Modified Eagle's Medium (DMEM) supplemented with a 5% of glutamine (200 mM), 10% fetal bovine serum (FBS), 5% penicillin (5000 units/cm^3) and streptomycin (5 mg/cm^3), at 37 °C in a 4% CO_2 atmosphere. Vero cells were disposed in a 96-weel culture plates (5000 cell/plate) in 0.2 cm^3 of DMEM medium. The medium was replaced, after 24 h, with another 0.2 cm^3 DMEM medium containing different concentrations of Nd-doped LaF_3 nanoparticles (0.5–500 μg/mm^3) and a negative control containing no nanoparticles (non-treated cells). Five replicates were performed per sample. After 24 incubation, the medium was removed and 0.02 cm^3 of MMT solution (0.5 mg/cm^3 in phosphate-buffered saline (PBS)) was added to each well. Finally, after incubation for 4 h formazan salt was dissolved with 0.2 cm^3 of dimethyl sulfoxide (DMSO) and the absorbance (Abs) was determined at λ = 570 nm on a microplate reader (Biotek ELX800). The relative cell viability (%) related to control wells containing cell culture medium without nanoparticles was calculated by [Abs]test/[Abs]control × 100.

Results and discussion

Morphology, size, and colloidal stability of Nd-doped LaF_3 Nanoparticles

As observed in the TEM images shown in Fig. 1, regardless of the Nd^{3+} doping level, all synthesized Nd-doped LaF_3 nanoparticles showed apparent spherical morphology with similar diameter (around 45 nm as determined from the histogram included in the figure). Nevertheless, a deeper observation of such micrographs revealed the presence of some elongated, higher contrast particles with a length similar to the diameter of the spherical particles and a thickness of 20 nm. This observation suggests that the samples consist of homogeneous, lenticular shape NPs, most of which were deposited with their rounded face parallel to the grid plane, giving rise to the spherical shapes, whereas some other fell down with that face perpendicular to the grid, leading to the observed elongated shapes.

DLS plots for all Nd-doped particles were very similar to those shown in Fig. 2, which correspond to the 2%Nd:LaF_3 sample, taken as a representative example. The hydrodynamic mean diameter obtained in aqueous solution (pH = 5.4) (Fig. 2) for this sample was 50 nm. This value was very similar to the mean diameter obtained from the TEM image, indicating that the synthesized nanoparticles are well dispersed, probably due to the presence of electrostatic repulsion forces on their surface, as indicated by the high value of zeta potential (+31 mV) measured for this sample.

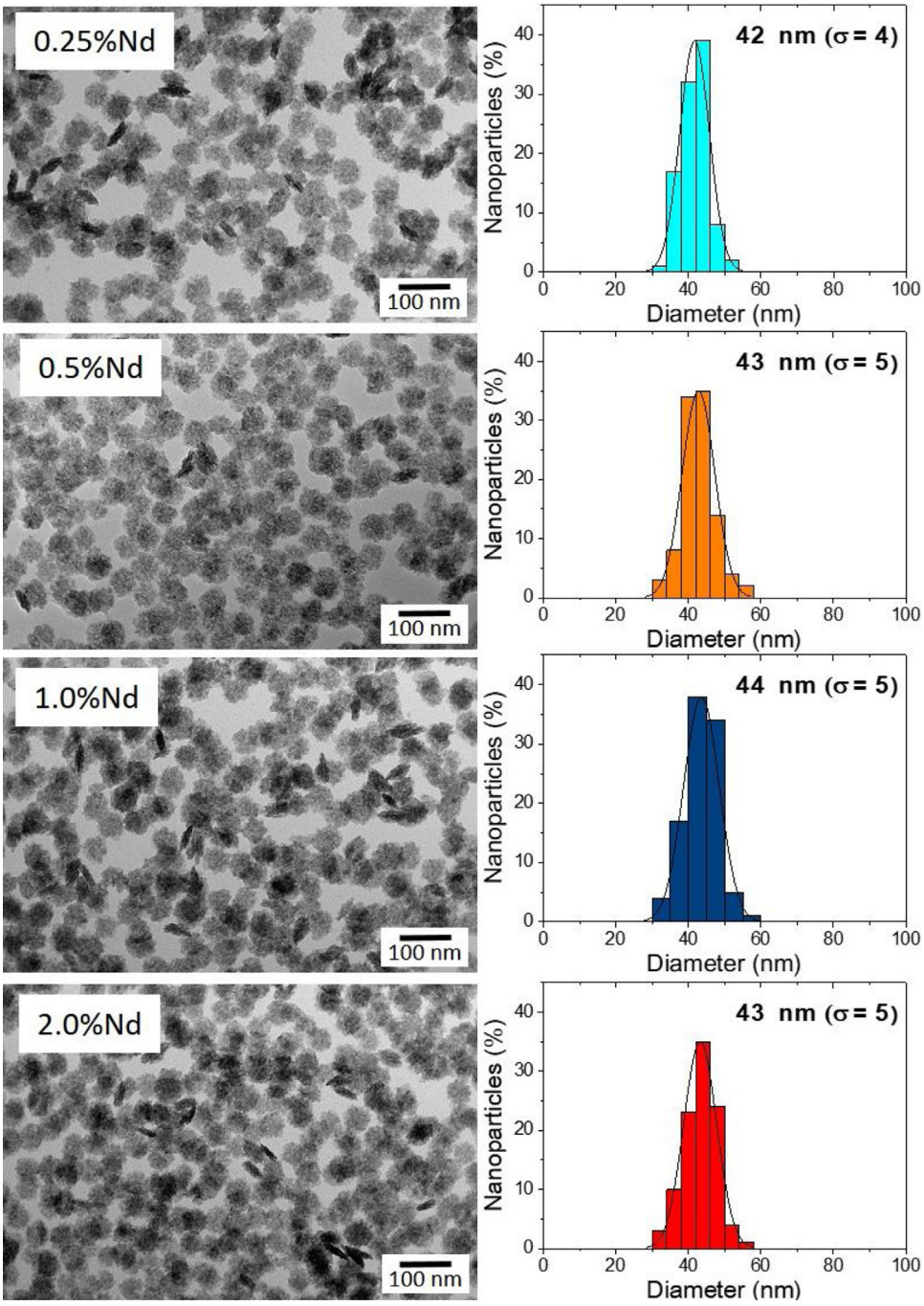

Fig. 1 – TEM micrographs (left) and the corresponding histograms showing size distribution (right) of the LaF_3 nanoparticles doped with different amounts of Nd^{3+}.

To obtain information about the colloidal stability of the Nd-doped LaF_3 nanoparticles in physiological media, they were dispersed in saline medium. In this case, the hydrodynamic diameter obtained (Fig. 2) was also very similar (57 nm) to that obtained from TEM indicating that the NPs were also colloidally stable in saline medium. The Nd:LaF_3 nanoparticles synthesized in this study meet, therefore, one of the most important requirements for their use *in vivo*.

X-ray diffraction

In spite of the low preparation temperature, all samples were crystalline as previously observed for the CeF_3 system synthesized by a similar procedure [24]. As shown in Fig. 3, the XRD patterns of all Nd-doped nanoparticles present a single set of reflections, which correspond to hexagonal lanthanum trifluoride (PDF 00-032-0483). This compound crystallizes in

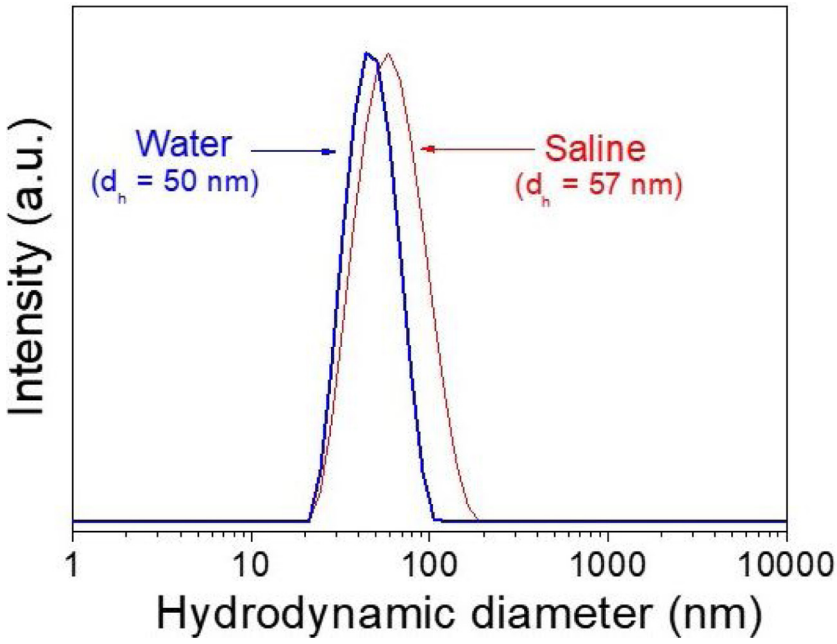

Fig. 2 – DLS plots showing hydrodynamic size distribution and mean hydrodynamic diameter (d_h) of 2%Nd:LaF_3 nanoparticles dispersed in water and saline medium.

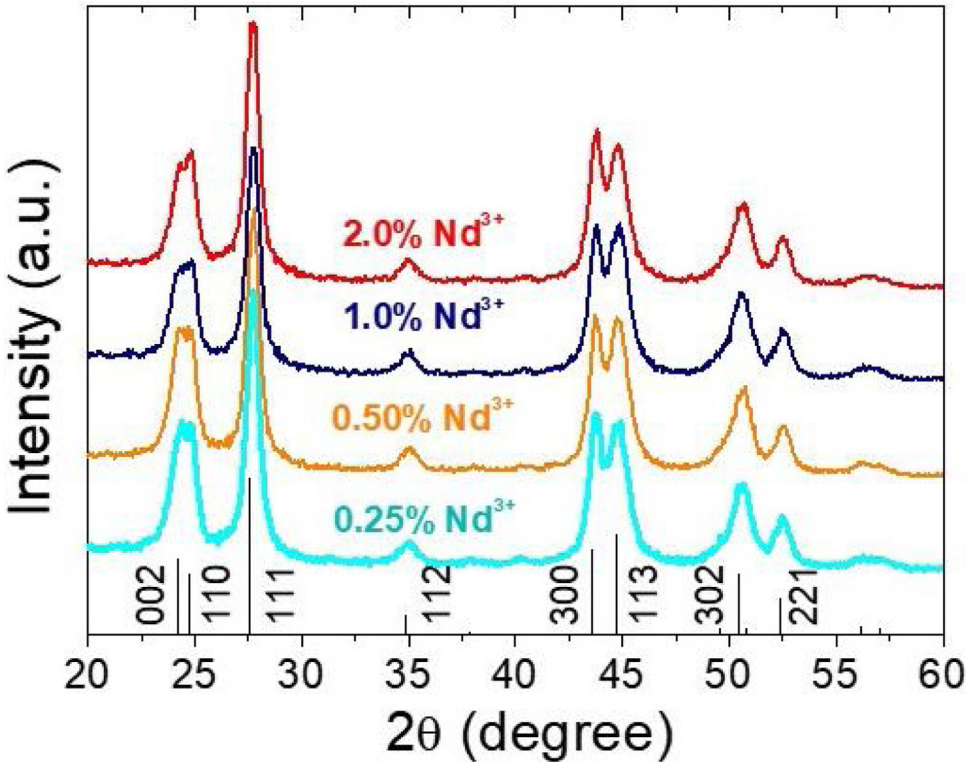

Fig. 3 – Experimental XRD patterns of LaF_3 nanoparticles doped with different amounts of Nd^{3+}. The hexagonal pattern of LaF_3 (ICDD No: 00-0032-0483) is shown at the bottom in black.

space group *P*−3*c*1. The La^{3+} cation is located at the center of a trigonal prism, with 6 fluorine atoms at the top and bottom corners and 3 fluorine atoms at the center of the faces, making a total of 9 F atoms coordinating La. The unit cell volume of the Nd:LaF_3 samples obtained with the Rietveld method (Table 1) showed a linear decrease with increasing Nd content. This result indicates the substitution of Nd^{3+} for La^{3+} in the LaF_3 hexagonal lattice as the ionic radius of Nd^{3+} (1.163 Å, in IX coordination) is smaller than that of La^{3+} (1.216 Å, in IX coordination). Finally, it is worth noting that the width of

Table 1 – Nominal and experimental composition, obtained by ICP, and unit cell volume, calculated by Rietveld refinement, of the Nd^{3+}-doped LaF_3 nanoparticles.

$Nd^{3+}/(Nd^{3+} + La^{3+})$		Unit cell volume (Å^3)
Nominal (%)	ICP (%)	
0.25	0.20	329.02
0.50	0.42	328.99
1.0	0.95	328.90
2.0	2.33	328.68

the reflections did not appreciably changed with Nd content, indicating a similar crystallinity degree for all doped samples.

Luminescent properties

Fig. 4a shows the excitation spectrum of the 2%Nd:LaF_3 NPs recorded by monitoring the emission at 1064 nm. The spectra of the other compositions analyzed in this study are qualitatively very similar to this one. This spectrum shows two broad features with maxima at 733 nm and 790 nm, which correspond to the electronic transitions in the Nd^{3+} 4*f* shell labeled in the figure. Excitation of the sample at 733 nm or 790 nm promotes electrons to the $^4F_{7/2}$ and $^4F_{5/2}$ excited states of Nd^{3+}, respectively, as shown in the 4*f* energy levels diagram of Nd^{3+} in Fig. 4c. The Nd^{3+} excited electrons then decay non-radiatively to the $^4F_{3/2}$ energy level from which they transit to the $^4I_{13/2}$, $^4I_{11/2}$ and $^4I_{9/2}$ states giving rise to the emission of infrared light with maxima at around 1320 nm, 1064 nm and 900 nm, respectively. The most intense emission, as observed in Fig. 4b, is located at 1064 nm, which is inside the biological window II. In this figure, an increase of the intensity of the emission spectra of the Nd:LaF_3 samples with increasing Nd doping level can be also observed, which must be attributed to the increase of the amount of Nd^{3+} emitting centers. This behavior is more clearly evidenced in Fig. 4d that shows the integrated area under the curve of the emission spectra corresponding to the different Nd-doped LaF_3 samples. Interestingly, such intensity increase was linear only at low Nd contents while a non-linear behavior was observed above 1% Nd. The emission intensity seems to reach its maximum value for a 2%Nd content. This finding is in agreement with previous observations carried out by Chen et al. for Nd-doped LaF_3 nanoparticles synthesized using oleic acid as capping agent [12]. Such evolution of the emission intensity is consistent with the presence of the well-known concentration quenching effect at high doping levels, when the emitting centers are close enough to each other

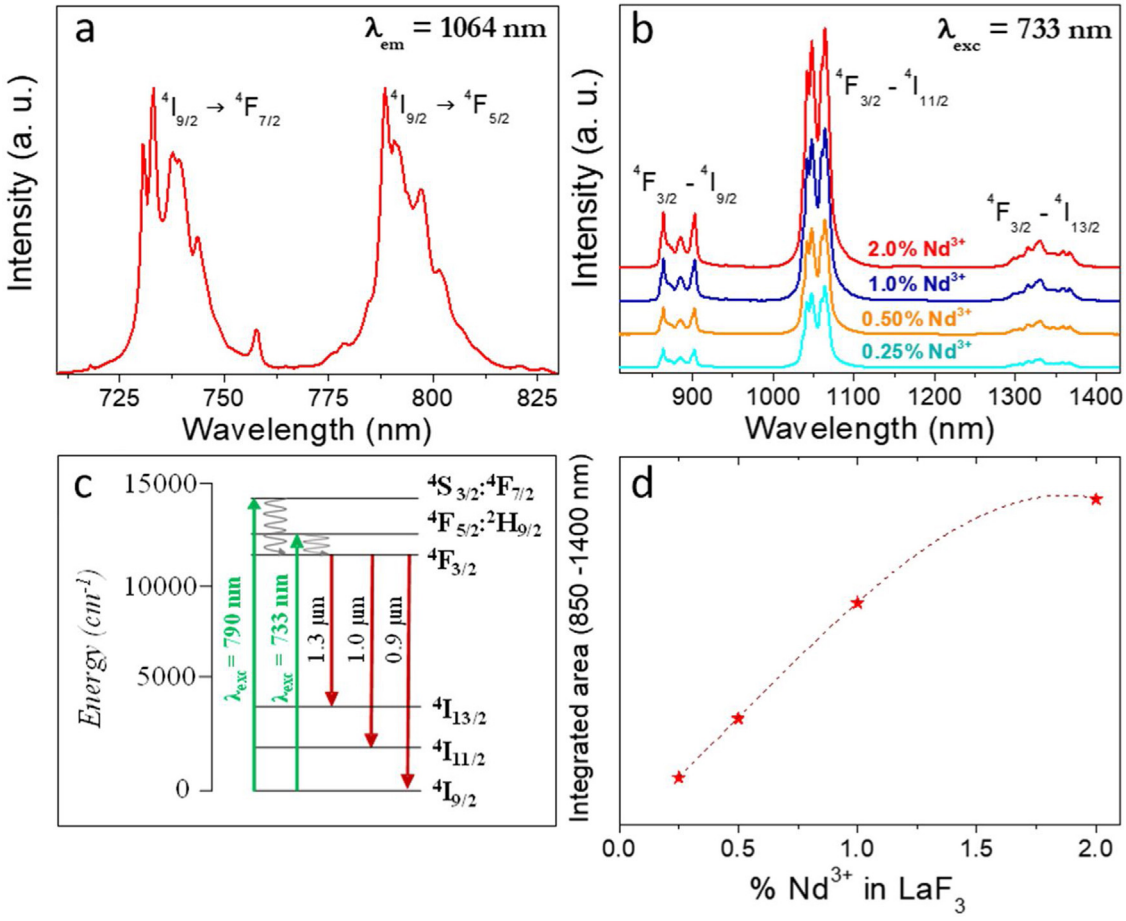

Fig. 4 – (a) Excitation spectrum of the 2%Nd^{3+}-doped LaF_3 sample. (b) Emission spectra of LaF_3 nanoparticles doped with different amounts of Nd^{3+}. (c) Nd^{3+} electronic energy levels diagram. (d) Integrated area between 850 and 1400 nm of the spectra shown in (b) versus Nd^{3+} concentration.

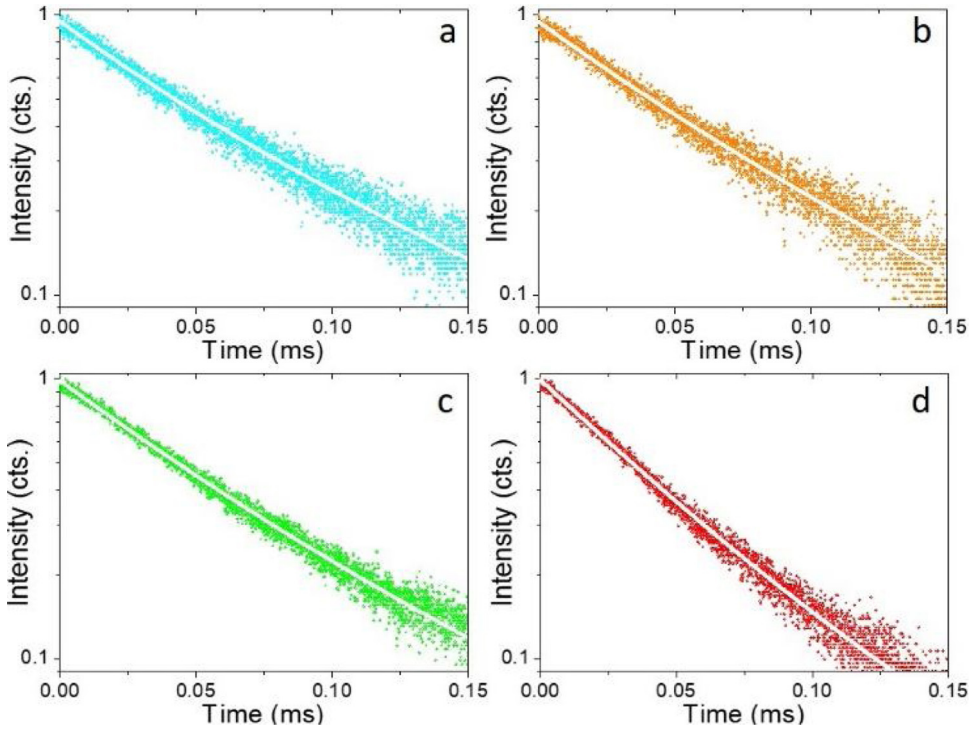

Fig. 5 – Temporal evolution of the $^4F_{3/2} \rightarrow {}^4I_{11/2}$ luminescence (1064 nm) for Nd^{3+}-doped LaF_3 nanoparticles having different doping levels: (a) 0.25%, (b) 0.5%, (c) 1.0% and (d) 2.0% (excitation at 532 nm using the second harmonics of a Nd:YAG laser).

as to enable energy transfer processes that eventually result in non-radiative emission and subsequent luminescence quenching [25,26].

Fig. 5 shows the luminescence decay curves recorded at an emission wavelength of 1064 nm for the different Nd-doped LaF_3 samples. All curves were successfully fitted to a biexponential decay of the form:

$$I(t) = I_1 \exp\left(\frac{-t}{\tau_1}\right) + I_2 \exp\left(\frac{-t}{\tau_2}\right) \quad [1]$$

where $I(t)$ is the luminescence intensity, t is the time after excitation, and τ_i ($i = 1, 2$) is the decay time of the i-component, with intensity I_i. This biexponential behavior has been usually observed for other lanthanide-based nanoparticulate systems [13,27] and arises from the presence of emitting centers in two different locations, namely, in the bulk (long component) and close to the NPs surface (short component) where the luminescence quenching by impurities and defects is more probable to occur. Table 2 presents the fitting parameters obtained from each curve together with the average decay time ($<\tau>$) calculated as:

$$\langle\tau\rangle = \frac{\int_0^\infty tI(t)dt}{\int_0^\infty I(t)dt} = \frac{\tau_1^2 I_1 + \tau_2^2 I_2}{\tau_1 I_1 + \tau_2 I_2} \quad [2]$$

It can be observed that the average decay time gradually decreases with increasing Nd content, the value for the 2%-doped sample being sensibly lower (53 μs) than the others (75–69 μs). This result agrees with previously reported observations [23] and confirms the concentration quenching behavior suggested by the evolution of the emission intensity vs. Nd doping level described above. In summary, it can be concluded that, although the most efficient sample is 0.25%Nd:LaF_3 because of its highest lifetime value, the most interesting sample from the application point of view is the one doped with 2%Nd as it shows the highest emission intensity.

Table 2 – Fitting parameters of the bi-exponential temporal dependence for the luminescence decay curves of the Nd^{3+}-doped nanoparticles (recorded at the dominant emission of Nd^{3+}) at different concentrations.

% Nd^{3+}	τ_1 (μs)	A_1 (%)	τ_2 (μs)	A_2 (%)	$<\tau>$ (μs)
0.25	60	78	107	22	75
0.5	60	79	100	21	72
1.0	60	84	100	15	69
2.0	50	96	100	4	53

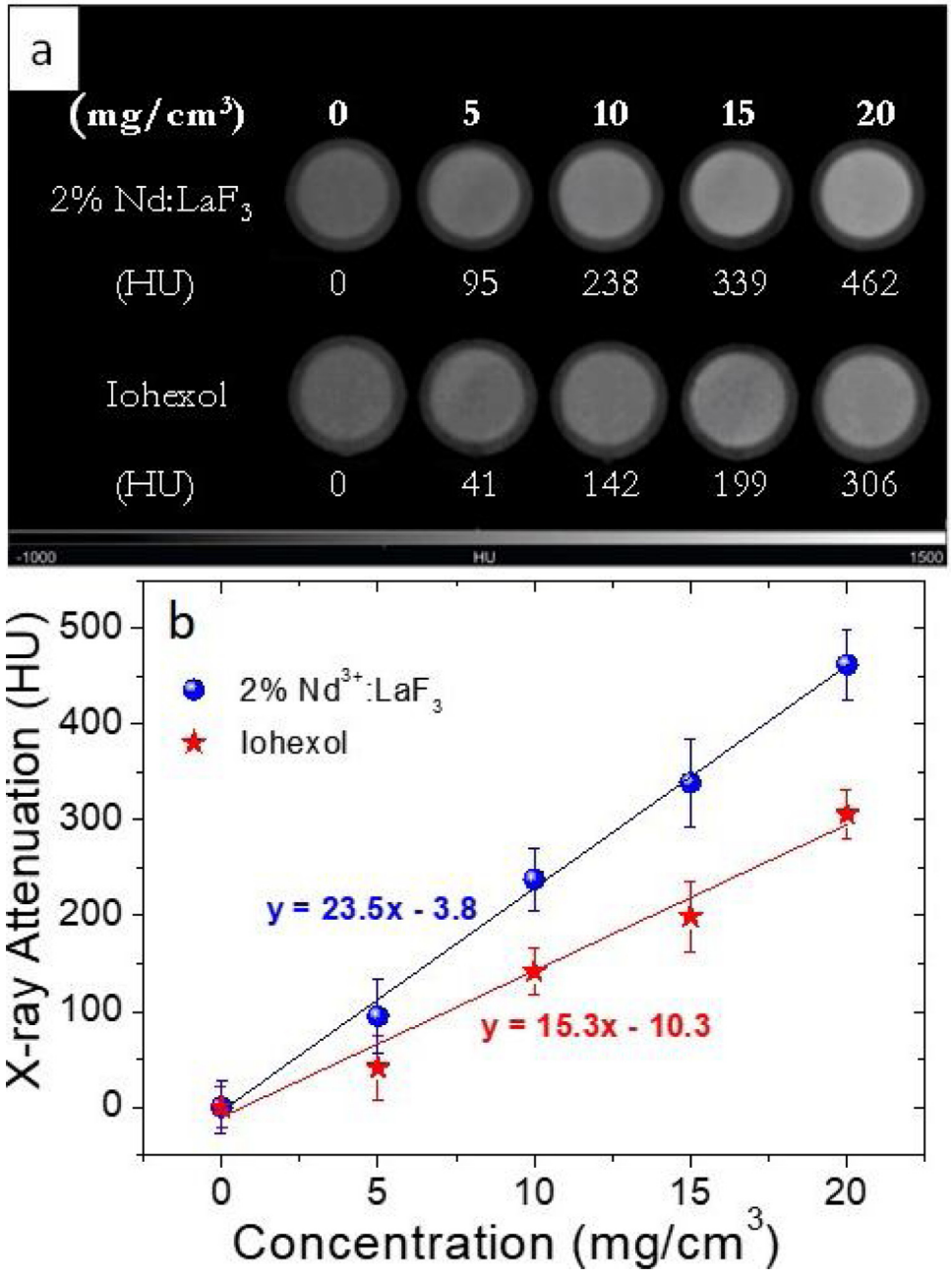

Fig. 6 – X-ray attenuation phantom images (a) and X-ray attenuation values in Hounsfield units (HU) (b) of aqueous suspensions having different concentration of 2%Nd^{3+}-doped LaF_3 nanoparticles and Iohexol.

X-ray attenuation capacity

The LaF_3 nanoparticles doped with 2%Nd were selected for the X-ray attenuation study for the reason given above. Fig. 6a shows the CT phantom images of aqueous suspensions with different concentration of 2%Nd:LaF_3 nanoparticles. The images obtained from aqueous solutions with the same concentration of a commercial CT CA (Iohexol) are also plotted in the figure for comparative purposes. It can be observed that the image contrast clearly increases with increasing NPs and Iohexol concentration, indicating the suitability of our NPs as CA for CT. We have also plotted the X-ray attenuation values, in Hounsfield units, obtained after processing the images shown above, versus the concentration of the CA for both the 2%Nd LaF_3 NPs and Iohexol (Fig. 6b). In both cases, the X-ray attenuation increases linearly with increasing CA concentration. However, the slope of the line corresponding to the Nd:LaF_3 NPs is significantly higher (23.5) than that shown by Iohexol (15.3), which indicates the higher X-ray attenuation capacity of the here developed probe.

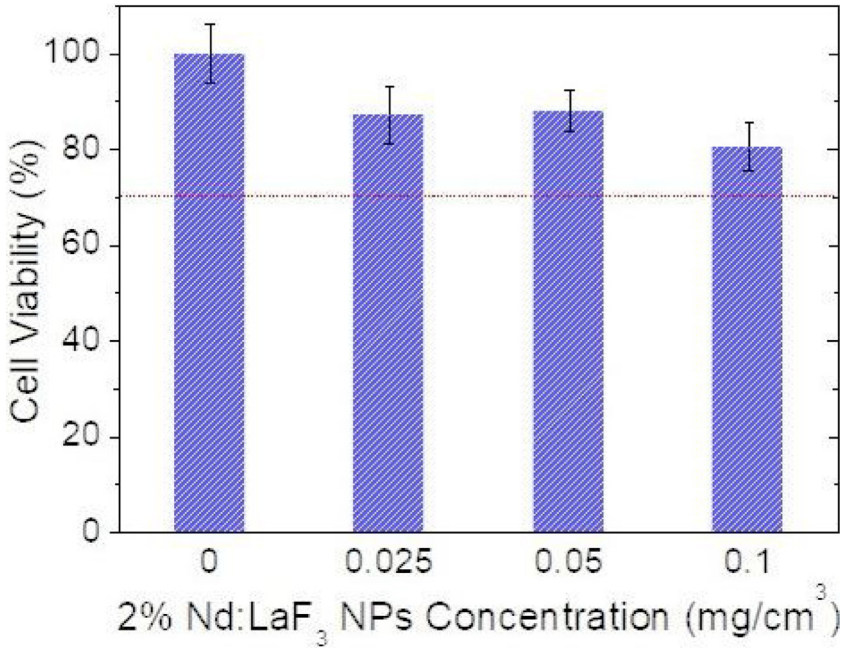

Fig. 7 – Cellular viability of the 2%Nd^{3+}-doped LaF_3 nanoparticles incubated with Vero cells for 24 h and determined by MTT assays. The percentage of viability of cells was expressed relative to control cells.

Cytotoxicity

The cytotoxicity of the Nd:LaF_3 NPs was analyzed by colorimetric MTT assay, following the methodology described in "Experimental" section, using Vero cells. The values obtained for cell survival, higher than 70% in all cases (Fig. 7) indicate that there is no significant cytotoxicity for NPs concentrations up to 0.1 mg/cm^3. This demonstrates that the here developed bimodal probe meets the biocompatibility requirement needed for its application in bioimaging.

Conclusions

Uniform neodymium-doped lanthanum trifluoride nanoparticles with hydrophilic character have been synthesized at room temperature by a homogeneous precipitation method in an ethylene glycol/water mixed solvent. The doped nanoparticles showed a lenticular shape with mean diameter around 45 nm, irrespective of the neodymium doping level. The luminescent properties of the synthesized samples were analyzed as a function of the Nd content to find the optimum phosphor. On excitation with near infrared light (λ = 733 nm), all samples displayed intense luminescence within the second biological window. Lifetime measurements revealed that the maximum luminescence efficiency was attained for the most diluted samples ($\leq$1% Nd^{3+}) since such magnitude decreased for the heavier doped sample (2%) as a consequence of concentration quenching. Nevertheless, the latter showed the strongest luminescence due to their higher content in luminescent centers, this sample being, therefore, the most interesting one from the application point of view. In addition, the X-ray attenuation capability of this phosphor has been evaluated for the first time in literature finding that it showed better attenuation properties than a commercial computed tomography contrast agent (Iohexol) indicating the superior suitability of the former for such imaging technique. Finally, the obtained nanoparticles were colloidally stable in saline medium and showed a high biocompatibility, meeting the mean requirements for their use in bioimaging applications.

Acknowledgements

Financial support was provided by the Spanish Ministry of Science, Innovation and Universities under grant RTI2018-094426-B-I00 (AEI/FEDER, UE), the Spanish Ministry of Science and Innovation under project PID2019-110632RB-I00 and Fondo Social de la DGA (grupos DGA). R.M. Calderón-Olvera thanks CONACYT-770734 postdoctoral grant. This work is dedicated to the memory of Victor M. Orera, a special scientist and a good friend.

REFERENCES

[1] S. Sivakumar, P.R. Diamente, F.C.J.M. van Veggel, Silica-coated Ln^{3+}-doped LaF_3 nanoparticles as robust down- and upconverting biolabels, Chem. Eur. J. 12 (2006) 5878–5884, http://dx.doi.org/10.1002/chem.200600224.
[2] S. Sivakumar, F.C.J.M. van Veggel, M. Raudsepp, Bright white light through up-conversion of a single NIR source from sol–gel-derived thin film made with Ln^{3+} doped LaF_3 nanoparticles, J. Am. Chem. Soc. 127 (2005) 12464–12465, http://dx.doi.org/10.1021/ja052583o.
[3] Y. Zhong, Q. Wang, G. Chen, Controllable preparation of carboxymethyl cellulose/LaF_3:Eu^{3+} composites and its application in anti-counterfeiting, Int. J. Biol. Macromol. 164

(2020) 2224–2231, http://dx.doi.org/10.1016/j.ijbiomac.2020.07.271.
[4] F.M. Xue, H.F. Wang, The stable and water-soluble neodymium-doped lanthanide fluoride nanoparticles for near infrared probing of copper ion, Talanta 99 (2012) 1057–1061, http://dx.doi.org/10.1016/j.talanta.2012.07.034.
[5] Y. Fan, Y. Wang, P. Wang, Z. Li, LaF_3 nanoparticle-assisted sensitive detection of protein kinase activity, Anal. Methods 6 (2014) 8621–8626, http://dx.doi.org/10.1039/c4ay01635a.
[6] E. Clayton Ximendes, W. Queiroz Santos, U. Rocha, U.K. Kagola, F. Sanz-Rodríguez, N. Fernández, A. da Silva Gouveia-Neto, D. Bravo, A. Martín Domingo, B. del Rosal, C.D.S. Brites, L. Dias Carlos, D. Jaque, C. Jacinto, Unveiling in vivo subcutaneous thermal dynamics by infrared luminescent nanothermometers, Nano Lett. 16 (2016) 1695–1703, http://dx.doi.org/10.1021/acs.nanolett.5b04611.
[7] M.S. Pudovkin, D.A. Koryakovtseva, E.V. Lukinova, S.L. Korableva, Sh.R. Khusnutdinova, A.G. Kiiamov, A.S. Nizamutdinov, V.V. Semashko, Luminescence nanothermometry based on Pr^{3+}: LaF_3 single core and Pr^{3+}: LaF_3/LaF_3 core/shell nanoparticles, Adv. Mater. Sci. Eng. (2019), http://dx.doi.org/10.1155/2019/2618307 [Article ID 2618307, 14 pages].
[8] M.H. Chen, Y.J. Jenh, S.K. Wu, Y.S. Chen, N. Hanagata, F.H. Lin, Non-invasive photodynamic therapy in brain cancer by use of Tb^{3+}-doped LaF_3 nanoparticles in combination with photosensitizer through X-ray irradiation: a proof-of-concept study, Nanoscale Res. Lett. 12 (2017) 62, http://dx.doi.org/10.1186/s11671-017-1840-3.
[9] R. Lv, G. Yang, F. He, Y. Dai, S. Gai, P. Yang, LaF_3:Ln mesoporous spheres: controllable synthesis, tunable luminescence and application for dual-modal chemo-/photo-thermal therapy, Nanoscale 6 (2014) 14799–14809, http://dx.doi.org/10.1039/c4nr04336g.
[10] M.C. Micheletto, E.J. Guidelli, A.J. Costa-Filho, Interaction of genetically encoded photosensitizers with scintillating nanoparticles for X-ray activated photodynamic therapy, ACS Appl. Mater. Interfaces 13 (2021) 2289–2302, http://dx.doi.org/10.1021/acsami.0c19041.
[11] U. Rocha, K.U. Kumar, C. Jacinto, I. Villa, F. Sanz-Rodríguez, M.C. Iglesias de la Cruz, A. Juarranz, E. Carrasco, F.C.J.M. van Veggel, E. Bovero, J. García Solé, D. Jaque, Neodymium-doped LaF_3 nanoparticles for fluorescence bioimaging in the second biological window, Small 10 (2014) 1141–1154, http://dx.doi.org/10.1002/smll.201301716.
[12] S. Cheng, L. Liu, Q. Yang, Y. Li, S. Zeng, In vivo optical bioimaging by using Nd-doped LaF_3 luminescent nanorods in the second near-infrared window, J. Rare Earths 37 (2019) 931–936, http://dx.doi.org/10.1016/j.jre.2018.11.014.
[13] D. González-Mancebo, A.I. Becerro, A. Corral, M. Moros, M. Balcerzyk, J.M. de la Fuente, M. Ocaña, Enhancing luminescence and X-ray absorption capacity of Eu^{3+}:LaF_3 nanoparticles by Bi^{3+}-codoping, ACS Omega 4 (2019) 765–774, http://dx.doi.org/10.1021/acsomega.8b03160.
[14] K. Chauhan, P. Sengar, K. Juarez-Moreno, G.A. Hirata, R. Vazquez-Duhalt, Camouflaged, activatable and therapeutic tandem bionanoreactors for breast cancer theranosis, J. Colloid Interface Sci. 580 (2020) 365–376, http://dx.doi.org/10.1016/j.jcis.2020.07.043.
[15] D. Jaque, C. Richard, B. Viana, K. Soga, X. Liu, J. García Solé, Inorganic nanoparticles for optical bioimaging, Adv. Opt. Photon. 8 (2016) 1–103, http://dx.doi.org/10.1364/AOP.8.000001.
[16] S.B. Yu, A.D. Watson, Metal-based X-ray contrast media, Chem. Rev. 99 (1999) 2353–2377, http://dx.doi.org/10.1021/cr980441p.
[17] A. Gnach, A. Bednarkiewicz, Lanthanide-doped up-converting nanoparticles: merits and challenges, Nano Today 7 (2012) 532–563, http://dx.doi.org/10.1016/j.nantod.2012.10.006.
[18] X. Duan, Y. Li, Physicochemical characteristics of nanoparticles affect circulation, biodistribution, cellular internalization, and tracking, Small 9 (2013) 1521–1532, http://dx.doi.org/10.1002/smll.201201390.
[19] F. Wang, Y. Zhang, X. Fan, M. Wang, Facile synthesis of water-soluble LaF_3:Ln^{3+} nanocrystals, J. Mater. Chem. 16 (2006) 1031–1034, http://dx.doi.org/10.1039/b518262j.
[20] J.W. Stouwdam, G.A. Hebbink, J. Huskens, F.C.J.M. van Veggel, Lanthanide-doped nanoparticles with excellent luminescent properties in organic media, Chem. Mater. 15 (2003) 4604–4616, http://dx.doi.org/10.1021/cm034495d.
[21] K. Cui, C. Gao, X. Cui, C. Hou, J. She, B. Peng, W. Wei, Effects of organic surfactant on fluorescence concentration quenching of Nd^{3+}-doped LaF_3 nanoparticles, Opt. Lett. 34 (2009) 2826–2828, http://dx.doi.org/10.1364/OL.34.002826.
[22] P.K. Nampoothiri, M.N. Gandhia, A.R. Kulkarni, Effect of surface grafting coefficient and chain length of fatty acids on the luminescence of neodymium^{3+}-doped LaF_3 nanoparticles, J. Mater. Chem. C 3 (2015) 1817–1822, http://dx.doi.org/10.1039/c4tc02646b.
[23] Y.V. Orlovskii, A.V. Popov, E.O. Orlovskaya, A.S. Vanetsev, E.A. Vagapova, M. Rähn, V. Sammelselg, I. Sildos, A.E. Baranchikov, P.V. Grachev, V.B. Loschenov, A.V. Ryabova, Comparison of concentration dependence of relative fluorescence quantum yield and brightness in first biological window of wavelengths for aqueous colloidal solutions of Nd^{3+}:LaF_3 and Nd^{3+}:KY_3F_{10} nanocrystals synthesized by microwave-hydrothermal treatment, J. Alloys Compd. 756 (2018) 182–192, http://dx.doi.org/10.1016/j.jallcom.2018.05.027.
[24] D. González-Mancebo, A.I. Becerro, T.C. Rojas, A. Olivencia, A. Corral, M. Balcerzyk, E. Cantelar, F. Cussó, M. Ocaña, Room temperature synthesis of water-dispersible Ln^{3+}:CeF_3 (Ln = Nd, Tb) nanoparticles with different morphology as bimodal probes for fluorescence and CT imaging, J. Colloid Interface Sci. 520 (2018) 134–144, http://dx.doi.org/10.1016/j.jcis.2018.03.007.
[25] Z.L. Wang, Z.W. Quan, P.Y. Jia, C.K. Lin, Y. Luo, Y. Chen, J. Fang, W. Zhou, C.J.O. Connor, J. Lin, A facile synthesis and photoluminescent properties of redispersible CeF_3, CeF_3:Tb^{3+}, CeF_3:Tb^{3+}/LaF_3 (core/shell) nanoparticles, Chem. Mater. 18 (2006) 2030–2037, http://dx.doi.org/10.1021/cm052360x.
[26] Y. Bu, X. Wang, X. Yan, Green–yellow–red tunable luminescence from Eu^{3+}–Ho^{3+}-doped TeO_2–GeO_2–Nb_2O_5 glass, Optoelectron. Adv. Mater. 7 (2013) 325–328.
[27] M. Laguna, N.O. Nuñez, A.I. Becerro, M. Ocaña, Morphology control of uniform $CaMoO_4$ microarchitectures and development of white light emitting phosphors by Ln doping (Ln = Dy^{3+}, Eu^{3+}), CrystEngComm 19 (2017) 1590–1600, http://dx.doi.org/10.1039/c6ce02611g.